Vibrational properties of MnO and NiO from DFT +U-based density functional perturbation theory

A. Floris, S. de Gironcoli, E. K. U. Gross, and M. Cococcioni

Phys. Rev. B **84**, 161102 — Published 13 October 2011

DOI: 10.1103/PhysRevB.84.161102

Vibrational properties of MnO and NiO from DFT+U-based Density Functional Perturbation Theory

A. Floris,[1,2] S. de Gironcoli,[3] E. K. U. Gross,[4,5] and M. Cococcioni[6]

[1] *Department of Physics, King's College London, London, Strand WC2R 2LS United Kingdom*
[2] *European Theoretical Spectroscopy Facility (ETSF)*
[3] *SISSA Condensed Matter Theory sector and CNR-IOM DEMOCRITOS Simulation Centre, via Bonomea 265, 34136 Trieste, Italy*
[4] *Max-Planck-Institut für Mikrostrukturphysik, Weinberg 2, D-06120 Halle, Germany*
[5] *European Theoretical Spectroscopy Facility (ETSF)*
[6] *Department of Chemical Engineering and Materials Science, University of Minnesota, 421 Washington Ave SE, Minneapolis, MN 55455, USA*

We introduce a novel extension of Density Functional Perturbation Theory (DFPT) that allows self-consistent linear-response calculations from a DFT+U ground state. Using this scheme, the full phonon dispersion of strongly correlated materials, whose ground state can be captured with Hubbard-corrected functionals, can be accessed with unprecedented accuracy and numerical efficiency. The new tool is applied to the study of MnO and NiO in their antiferromagnetic (AFII) ground state. Our results confirm the highly non-cubic behavior of these systems and show a strong interplay between features of the phonon spectrum and the occupation of specific d states, suggesting the possibility to investigate the electronic structure of these materials through the analysis of their phonon spectrum.

Late transition-metal (TM) monoxides (MnO, FeO, CoO, NiO), the prototypes of strongly correlated systems, are well-known to be poorly described by density functional theory (DFT) within the commonly used approximate functionals, such as LDA and GGA. Their insulating AFII state, however, can be captured quite accurately by the popular DFT+U[1] scheme[2–5], based on a Hubbard-model additive correction to the DFT Hamiltonian[6–11]. In this paper we exploit the DFT+U improved description of the electronic ground state of these systems to accurately compute their vibrational properties.

In the last decades the lattice vibrations of TM monoxides have been investigated quite intensively with experimental techniques[12–16]. Calculations, however, have been more sparse[17–22] and, with the exception of Ref.[18] (a Green-function-based method from a DFT+DMFT functional), none of them was based on linear response theory, which is computationally much more efficient than methods requiring a supercell (e.g., "frozen-phonon").

In this article we extend the formulation of Density Functional Perturbation Theory (DFPT)[23] to the DFT+U Hamiltonian. This allows calculations of the entire vibrational spectrum of the DFT+U ground state of correlated materials with unprecedented accuracy and efficiency. Moreover, by computing the Hubbard U through the linear-response method of Ref.[24], our scheme is completely parameter-free. "DFPT+U" numerical results will be shown for MnO and NiO in their antiferromagnetic (low temperature) phase. The two GGA+U vibrational spectra will be analyzed in detail and compared with GGA results and with available experimental data.

DFPT is based on the application of first-order perturbation theory to the ground state of the self-consistent Kohn-Sham (KS) Hamiltonian (see Ref.[23], Sec. II.C, whose notation is adopted in the following). The displacement of an ion L in direction α from its equilibrium position induces a perturbation $\Delta^\lambda V_{SCF}$ in the electronic KS potential V_{SCF}, leading to a variation $\Delta^\lambda n(r)$ of the charge density ($\lambda \equiv \{L\alpha\}$). Since the Hubbard *potential* V_{Hub} is a corrective addition to the KS potential, its variation $\Delta^\lambda V_{Hub}$ must be added to $\Delta^\lambda V_{SCF}$ when solving the DFPT equations[23]. The V_{Hub} expression reads[5]:

$$V_{Hub} = \sum_{I\sigma mm'} U^I \left[\frac{\delta_{mm'}}{2} - n^{I\sigma}_{mm'}\right] |\varphi^I_{m'}\rangle\langle\varphi^I_m|. \qquad (1)$$

In Eq. (1), the atomic occupations $n^{I\sigma}_{mm'}$ are computed projecting the KS states $|\psi^\sigma_i\rangle$ on atomic orbitals $|\varphi^I_m\rangle$, i.e. $n^{I\sigma}_{mm'} = \sum_i^{occ} \langle\psi^\sigma_i|\varphi^I_m\rangle\langle\varphi^I_{m'}|\psi^\sigma_i\rangle$; I and m represent indexes of the atomic site and state, respectively[24]. The linear-response of the Hubbard potential then reads:

$$\begin{aligned}\Delta^\lambda V_{Hub} = &\sum_{I\sigma mm'} U^I \left[\frac{\delta_{mm'}}{2} - n^{I\sigma}_{mm'}\right] \times \\ &\left[|\Delta^\lambda\varphi^I_{m'}\rangle\langle\varphi^I_m| + |\varphi^I_{m'}\rangle\langle\Delta^\lambda\varphi^I_m|\right] - \\ &\sum_{I\sigma mm'} U^I \Delta^\lambda n^{I\sigma}_{mm'} |\varphi^I_{m'}\rangle\langle\varphi^I_m| \qquad (2)\end{aligned}$$

where $\Delta^\lambda\varphi^I_m$ is the response of the atomic wavefunction φ^I_m due to a shift in the position of its center and

$$\begin{aligned}&\Delta^\lambda n^{I\sigma}_{mm'} = \qquad (3)\\ &\sum_i^{occ}\{\langle\psi^\sigma_i|\Delta^\lambda\varphi^I_m\rangle\langle\varphi^I_{m'}|\psi^\sigma_i\rangle + \langle\psi^\sigma_i|\varphi^I_m\rangle\langle\Delta^\lambda\varphi^I_{m'}|\psi^\sigma_i\rangle\} \\ &+ \sum_i^{occ}\{\langle\Delta^\lambda\psi^\sigma_i|\varphi^I_m\rangle\langle\varphi^I_{m'}|\psi^\sigma_i\rangle + \langle\psi^\sigma_i|\varphi^I_m\rangle\langle\varphi^I_{m'}|\Delta^\lambda\psi^\sigma_i\rangle\}.\end{aligned}$$

Note that, in Eq. (2), the terms arising from the variation $\Delta^\lambda U^I$ are assumed to be negligible. In Eq. (3), $|\Delta^\lambda\psi^\sigma_i\rangle$ is

the KS state linear response to the atomic displacement, computed solving the DFPT equations ([23], Sec. II.C).

Once the density response $\Delta^\lambda n(r) = 2Re\sum_{i\sigma}^{occ}\psi_i^{*\sigma}\Delta^\lambda\psi_i^\sigma$ is obtained, the dynamical matrix can be constructed and the phonon frequencies and vibrational modes are calculated. However, the Hubbard *energy* correction $E_{Hub} = \frac{1}{2}\sum_{I\sigma mm'} U^I(\delta_{mm'} - n^{I\sigma}_{mm'})n^{I\sigma}_{mm'}$ will contribute to the standard (LDA/GGA) dynamical matrix with the following additional term:

$$\Delta^\mu\left(\partial^\lambda E_{Hub}\right) = \sum_{I\sigma mm'} U^I\left[\frac{\delta_{mm'}}{2} - n^{I\sigma}_{mm'}\right]\Delta^\mu\left(\partial^\lambda n^{I\sigma}_{mm'}\right) - \sum_{I\sigma mm'} U^I\Delta^\mu n^{I\sigma}_{mm'}\partial^\lambda n^{I\sigma}_{mm'}, \quad (4)$$

namely the total derivative of the Hubbard contribution $\partial^\lambda E_{Hub}$ to Hellmann-Feynman forces[25]. In Eq. (4), ∂^λ indicates a *bare* derivative, i.e. taken at fixed orbitals ψ_i^σ[26]. Finally, in case of insulators and semiconductors, a "non analytical" term $C^{na}_{I\alpha,J\beta}$ must be added to the dynamical matrix to account for the coupling of longitudinal vibrations with the macroscopic electric field generated by ionic displacements. This term, responsible for the LO-TO splitting at $\mathbf{q} = \Gamma$, depends on the Born effective-charge tensor $\mathbf{Z}^*$ and the high-frequency electronic dielectric tensor ϵ^∞: $C^{na}_{I\alpha,J\beta} = \frac{4\pi e^2}{\Omega}\frac{(\mathbf{q}\cdot\mathbf{Z}^*_I)_\alpha(\mathbf{q}\cdot\mathbf{Z}^*_J)_\beta}{\mathbf{q}\cdot\overleftrightarrow{\epsilon}^\infty\cdot\mathbf{q}}$[27]. The calculation of $\mathbf{Z}^*_{I,\alpha\beta}$ and $\epsilon^\infty_{\alpha\beta}$ is based on the response of the electronic system to a macroscopic electric field and requires the evaluation of the transition amplitudes between valence and conduction KS states promoted by the commutator of the KS Hamiltonian with the position operator $\mathbf{r}$, $\langle\psi_{c,\mathbf{k}}|\left[H_{SCF},\mathbf{r}\right]|\psi_{v,\mathbf{k}}\rangle$[28]. A finite contribution to this quantity comes from the presence of the (non-local) Hubbard potential:

$$\langle\psi^\sigma_{c,\mathbf{k}}|\left[V^\sigma_{Hub},r_\alpha\right]|\psi^\sigma_{v,\mathbf{k}}\rangle = \sum_{Imm'} U^I\left[\frac{\delta_{mm'}}{2} - n^{I\sigma}_{mm'}\right] \times\left[-i\langle\psi^\sigma_{c,\mathbf{k}}|\frac{d}{dk_\alpha}\left(|\varphi^I_{m,\mathbf{k}}\rangle\langle\varphi^I_{m',\mathbf{k}}|\right)|\psi_{v,\mathbf{k}}\rangle\right] \quad (5)$$

where $\varphi^I_{m,\mathbf{k}}$ are Bloch sums of atomic wavefunctions and k_α is a component of the Bloch vector $\mathbf{k}$.

To summarize, the extension of DFPT to the DFT+U functional amounts to the definition and implementation of *three* contributions: *i)* the variation of the Hubbard potential $\Delta^\lambda V_{Hub}$ to be added to $\Delta^\lambda V_{SCF}$; *ii)* the second derivative $\Delta^\mu\left(\partial^\lambda E_{Hub}\right)$ to be added to the analytical part of the dynamical matrix; *iii)* a term to the "non analytical" dynamical matrix.

This DFPT extension was implemented in the PHONON code of the QUANTUM ESPRESSO package[29]. Although the formalism presented above is valid only for norm-conserving (NC) pseudopotentials and for insulators, our implementation has been extended to ultrasoft (US) pseudopotentials[26,30] and metallic systems. The corresponding formal extension, crucial for efficient calculations of systems with localized electrons, will be presented in a future publication.

We now discuss the phonon spectrum of MnO and NiO, obtained with this novel approach[31]. The U^I values were determined via the linear-response approach of Ref.[24], leading to $U^{Mn} = 5.25$ eV and $U^{Ni} = 5.77$ eV.

MnO and NiO crystallize in the cubic rock-salt structure but acquire a rhombohedral symmetry due to their antiferromagnetic order consisting of ferromagnetic (111) planes of cations alternating with opposite magnetization. DFT+U has been used quite successfully to characterize this AFII ground state[6,10].

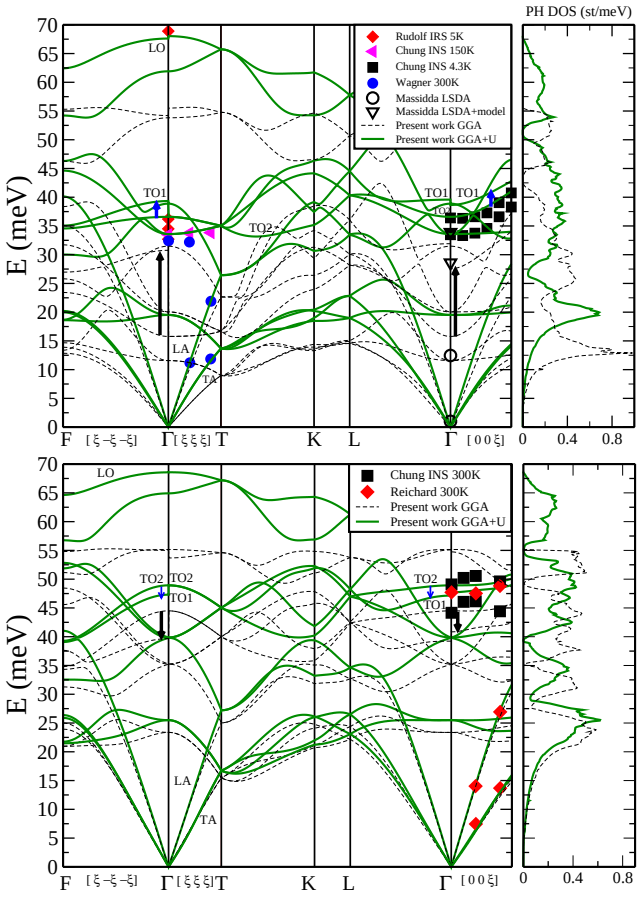

FIG. 1. (Color online) MnO (upper panel) and NiO (lower) phonon dispersion, calculated in GGA (dashed lines) and GGA+U (solid thick lines). Blue (black) arrows mark the GGA+U (GGA) magnetic splittings and their sign (see text). Upper panel: Filled symbols represent experimental data[12,13,15], open symbols the results of other calculations (at zone-center)[17]. Lower panel: Symbols represent experimental data[12,16]. Note that for NiO the arrows point downwards, to indicate the sign difference with respect to MnO. Right panels: phonon DOS.

Fig. 1 (up) shows the MnO phonon dispersion calculated with GGA and GGA+U. The most evident effect brought about by the Hubbard correction is a general upward shift of the frequencies, making the GGA+U spectrum in much better agreement than GGA with available experiments[12,13,15], for both acoustic and optical branches (also confirming the accuracy of the linear-

response calculation[24] of the Hubbard parameter). Note, in particular, the considerable improvement over GGA in the calculation of LO and TO frequencies at $\mathbf{q} = \Gamma$ (GGA underestimates the LO frequency by ≈ 15 meV). The frequency shift is clearly illustrated in the phonon DOS (Fig. 1, right panel), exhibiting also a different weight distribution, with a more disperse structure in the GGA+U case. A second noteworthy change consists in the substantial reduction of the splitting between the TO modes in the $[1\bar{1}\bar{1}]$ and [001] directions. Along these directions, the discontinuous and continuous modes at the zone center are indicated as TO1 and TO2 and correspond to counter-phase vibrations of the Mn and O sub-lattices. Both transverse optical modes along [111] are polarized in the (111) ferromagnetic planes. Along $[1\bar{1}\bar{1}]$ and [001] directions, the transverse mode TO2 also vibrates parallel to the (111) planes and is continuous at $\mathbf{q} = \Gamma$. Transverse mode TO1, instead, vibrates out of these planes for $\mathbf{q} \in [1\bar{1}\bar{1}]$ and $\mathbf{q} \in [001]$ (along [211] and [110], respectively) and the inequivalence between {111} planes due to magnetism causes the TO1 to be discontinuous and to split from TO2. A similar effect, although less pronounced, can also be observed for LO modes. These splittings are absent in the paramagnetic cubic phase[20]. In fact, as pointed out by Massidda *et al.*[17], the TO splitting has a purely magnetic origin.

The splitting reduction was interpreted in Ref.[17] as a consequence of the suppression of the Mn-O hybridization, produced by the stronger localization of d states due to the Hubbard correction. The latter also results in a concomitant increase of the KS electronic band-gap. An alternative, albeit equivalent, way to understand the magnetic splitting reduction is through the super-exchange mechanism, expected to be responsible for the magnetic coupling J between metal ions[32–35]. In fact, according to second-order perturbation theory, $J \propto t^2/\Delta$, where t is the hopping amplitude between d and p states and Δ is their energy separation. A larger U destabilizes empty (minority spin) d states, resulting in a substantial increase of Δ and a reduction of J.

The phonon dispersion of NiO is presented in Fig. 1 (lower panel). Overall, NiO shows the same trends observed in MnO: The Hubbard correction shifts the frequencies upward (in a less pronounced way than in MnO) improving the agreement with experiments[12,36]. Also for NiO the magnetic splitting Δ_{TO} significantly contracts in comparison to GGA. At variance with MnO, however, TO1 splits *downward* along the [001] and the $[1\bar{1}\bar{1}]$ directions, appearing softer than TO2. In Ref.[19] the splitting Δ_{TO} (and, in particular, its sign) has been related to the magnetic coupling between metal ions according to the formula $\Delta_{TO} = \frac{d^2 J_1}{dQ_x dQ_y}$, where Q_x and Q_y are atomic displacements along two directions parallel to the side of the cubic cell. Thus, a change in the sign of the nearest-neighbor magnetic coupling J_1, as found in Ref.[19], could be responsible for the inverted order of TO1 and TO2. While this is consistent with the experimental results from Ref.[36], it seems in contrast with the ones of Chung *et al.*[12] (believed to be "more controversial"[19]) who do not observe a sign change in the splittings of NiO and MnO. Our results confirm those of Ref.[19]. We notice, moreover, that the sign of Δ_{TO} correlates with the occupation of specific subsets of orbitals, namely the minority spin e_g states. At ambient pressure, the metal ions of all late TM monoxides have maximum magnetization, with five electrons in the majority spin d orbitals and the rest in the minority spin counterparts. From MnO to NiO the number of minority spin d electrons varies from 0 to 3 (FeO has 1, CoO has 2). The d states of TM ions in octahedral coordination with O, as in these compounds, are subjected to a crystal field that splits them into a doublet (e_g) and a triplet (t_{2g}), with the latter at lower energy. e_g states point along the TM-O directions, while the t_{2g} are directed towards the mid point of the sides of the oxygen octahedra. The AFII-induced rhombohedral symmetry further splits the t_{2g} triplet in a second doublet (e'_g) with e_g symmetry and a lone state a_{1g} that corresponds to a z^2 state along the [111] cubic diagonal. In MnO the minority spin states, nominally empty, show a residual occupation (due to the incomplete transfer of electrons from the Mn to the O) that mostly concentrates on the e_g states. NiO, instead, has nominally 3 minority-spin electrons mostly concentrated on t_{2g} (e'_g and a_{1g}) states, with higher-energy e_g states almost empty. Going from MnO to NiO, as the occupation of the minority-spin states increases, t_{2g} orbitals become more and more stable and their occupation eventually becomes larger than that of e_g states. We argue that the Δ_{TO} change of sign is related to this cross-over. In fact, when minority-spin e_g states are more occupied, more electronic charge is concentrated in the TM-O "bonds", making them stronger and increasing the frequency of the TO1 mode. When t_{2g} states are occupied, instead, the electronic charge points towards interstitial spaces and the energy required by the TO1 vibration of the two sublattices against each other along directions oblique to the (111) planes is lower than that of vibrations parallel to these planes (TO2) that bring t_{2g} states to partially overlap with oxygen p orbitals. While not strictly quantitative, this scenario seems consistent with what was observed in some Fe compounds under pressure, where the transition from a high-spin state to a low-spin one (with the conversion of the majority e_g electrons into minority t_{2g} manifold) is accompanied by a significant softening of the bulk modulus[37]. Further calculations (not presented here) on CoO (2 minority-spin electrons) and CoO^+ (1 minority-spin electron) confirm this interpretation: while CoO (with low-lying occupied e'_g, and essentially unoccupied e_g) behaves like NiO, CoO^+ (with a_{1g} occupied and e_g partially occupied) has a splitting of the same sign as MnO. The occupation of the minority e_g states can also be related to the change in the sign of J_1 through super-exchange theory[32–35]: lower occupations of these orbitals increase the weight of virtual transitions to them and make the interactions more strongly negative (ferromagnetic). In this view, the change of sign of

J_1 and of the magnetic splitting can be regarded as consequences of the redistribution of electrons on the TM d states. A detailed study of the vibrational properties of strongly correlated materials can therefore shed light on their electronic structure and magnetic interactions.

To summarize: In this work we have introduced an extension of DFPT allowing linear response calculations from a DFT+U ground state. The scheme represents a highly efficient method to calculate the entire vibrational spectrum of systems with strong electronic correlation. The approach exploits two computational advantages of DFPT and DFT+U: *i)* the possibility to avoid supercell calculations and *ii)* the affordable cost of the Hubbard correction in the calculations of the total energy and its derivatives. The excellent agreement with experimental measurements obtained for MnO and NiO demonstrates the accuracy of the new computational tool. In addition, the results suggest the possibility to investigate fine details of the electronic structure of these materials through their signature on the vibrational spectrum. The methodological extension introduced in this work will be crucial to study the behavior of TM compounds at finite temperature and in studies requiring a highly accurate vibrational spectrum, e. g. calculations of the electron-phonon coupling in high-T_c superconductors.

Acknowledgments We thank Sandro Massidda for useful discussions. This work was supported by the Deutsche Forschungsgemeinschaft through SPP11 and by the NSF grant EAR-0810272. The authors are also grateful to the Minnesota Supercomputing Institute for providing computational resources that were used for part of the calculations presented in this paper.

[1] DFT+U will indicate LDA+U or GGA+U, according to the approximate DFT functional used.
[2] J. Z. V. I. Anisimov and O. K. Andersen, Phys. Rev. B **44**, 943 (1991).
[3] V. I. Anisimov, I. S. Elfimov, N. Hamada, and K. Terakura, Phys. Rev. B **54**, 4387 (1996).
[4] V. I. Anisimov, F. Aryasetiawan, and A. I. Lichtenstein, J. Phys.: Condens. Matter **9**, 767 (1997).
[5] S. L. Dudarev, G. A. Botton, S. Y. Savrasov, C. J. Humphreys, and A. P. Sutton, Phys. Rev. B **57**, 1505 (1998).
[6] O. Bengone, M. Alouani, P. Blöchl, and J. Hugel, Phys. Rev. B **62**, 16392 (2000).
[7] T. Tsuchiya, R. M. Wentzcovitch, C. R. S. da Silva, and S. de Gironcoli, Phys. Rev. Lett. **96**, 198501 (2006).
[8] W.-B. Zhang, Y.-H. Deng, Y.-L. Hu, K.-L. Han, and B.-Y. Tang, Solid State Communications **142**, 6 (2007).
[9] T. Cai, H. L. Han, Y. Yu, T. Gao, J. G. Du, and L. H. Hao, Physica B-Condensed Matter **404**, 89 (2009).
[10] V. L. Campo Jr and M. Cococcioni, Journal of Physics: Condensed Matter **22**, 055602 (2010).
[11] K. Karlsson, F. Aryasetiawan, and O. Jepsen, Phys. Rev. B **81**, 245113 (2010).
[12] E. M. L. Chung, D. M. Paul, G. Balakrishnan, M. R. Lees, A. Ivanov, and M. Yethiraj, Phys. Rev. B **68**, 140406 (2003).
[13] T. Rudolf, C. Kant, F. Mayr, and A. Loidl, Phys. Rev. B **77**, 024421 (2008).
[14] B. C. Haywood and M. F. Collins, Journal of Physics C: Solid State Physics **4**, 1299 (1971).
[15] V. Wagner, W. Reichardt, and K. W., Proc. Conf. Neutron Scattering **1**, 175 (1976).
[16] W. Reichardt, V. Wagner, and W. Kress, Journal of Physics C: Solid State Physics **8**, 3955 (1975).
[17] S. Massidda, M. Posternak, A. Baldereschi, and R. Resta, Phys. Rev. Lett. **82**, 430 (1999).
[18] S. Y. Savrasov and G. Kotliar, Phys. Rev. Lett. **90**, 056401 (2003).
[19] W. Luo, P. Zhang, and M. L. Cohen, Solid State Communications **142**, 504 (2007).
[20] U. D. Wdowik and D. Legut, Journal of Physics: Condensed Matter **21**, 275402 (2009).
[21] Y. Wang, J. E. Saal, J.-J. Wang, A. Saengdeejing, S.-L. Shang, L.-Q. Chen, and Z.-K. Liu, Phys. Rev. B **82**, 081104 (2010).
[22] S. Y. Park and H. J. Choi, Phys. Rev. B **80**, 155122 (2009).
[23] S. Baroni, S. de Gironcoli, A. Dal Corso, and P. Giannozzi, Rev. Mod. Phys. **73**, 515 (2001).
[24] M. Cococcioni and S. de Gironcoli, Phys. Rev. B **71**, 35105 (2005).
[25] M. Cococcioni, Reviews in Mineralogy & Geochemistry **71**, 147 (2010).
[26] A. Dal Corso, Phys. Rev. B **64**, 235118 (2001).
[27] W. Cochran and R. A. Cowley, Journal of Physics and Chemistry of Solids **23**, 447 (1962).
[28] P. Giannozzi, S. de Gironcoli, P. Pavone, and S. Baroni, Phys. Rev. B **43**, 7231 (1991).
[29] P. Giannozzi *et al.*, Journal of Physics: Condensed Matter **21**, 395502 (2009).
[30] D. Vanderbilt, Phys. Rev. B **41**, 7892 (1990).
[31] Calculations were performed at the experimental constants for both materials, in their cubic undistorted structure. We used Ultrasoft pseudopotentials with a GGA-PBE xc functional[38]. A wavefunction (charge) energy cut-off of 60Ry (600Ry) and a Monkhorst-Pack grid of 10^3 **k**-points for scf and phonon calculations were sufficient to converge all the modes within 3%. Phonon dispersions were obtained interpolating from a 4×4×4 grid of **q** vectors.
[32] P. W. Anderson, Phys. Rev. **79**, 350 (1950).
[33] J. B. Goodenough, J. Phys. Chem. Solids **6**, 287 (1958).
[34] P. W. Anderson, Phys. Rev. **115**, 2 (1959).
[35] J. Kanamori, J. Phys. Chem. Solids **10**, 87 (1959).
[36] M. T. Hutchings and E. J. Samuelsen, Phys. Rev. B **6**, 3447 (1972).
[37] H. Hsu, P. Blaha, M. Cococcioni, and R. M. Wentzcovitch, Phys. Rev. Lett. **106**, 118501 (2011).
[38] J. P. Perdew, K. Burke, and M. Ernzheroff, Phys. Rev. Lett. **77**, 3865 (1996).